# Using magnetic fluids to simulate convection in a central force field in the laboratory

Nonlinear Processes in Geophysics, 12, 877–889, 2005
SRef-ID: 1607-7946/npg/2005-12-877
European Geosciences Union


Nonlinear Processes in Geophysics

# Using magnetic fluids to simulate convection in a central force field in the laboratory

**W.-G. Früh**

School of Engineering and Physical Sciences, Heriot Watt University, Riccarton, Edinburgh, EH14 4AS, UK

Received: 22 August 2005 – Revised: 25 October 2005 – Accepted: 25 October 2005 – Published: 3 November 2005

Part of Special Issue "Turbulent transport in geosciences"

**Abstract.** Large-scale convection in planetary or stellar interiors plays a significant role but it is difficult to reproduce the central force field of those systems in experimental studies. A technique to approximate a central force field through the magnetic field from magnets acting on a magnetic liquid is presented. The thermomagnetic convection in a spherical shell filled with a magnetic liquid is analyzed in the context of a terrestrial laboratory using a 2D Finite Element model. Two configurations of magnetic fields were investigated, one resulting in a radially decreasing force field, and the other in a radially increasing force field.

The results suggest that, while the actual force field does not reproduce the central gravity in planetary interiors accurately, it captures the essential qualitative character of the flow unlike other terrestrial experiments, which were either dominated by gravity or by a cylindrical radial force field. It is therefore suggested that such an experiment would provide a useful tool to investigate thermal convection in planetary interiors.

## 1 Introduction

Large-scale convection in planetary or stellar interiors plays a significant role both in the transport of heat from the deep interior to the planet's or star's surface, e.g. Huppert (2000), as well as the generation of the planetary magnetic fields by geodynamo actions, e.g. Moffatt (2000). To simulate this process in the laboratory is problematic as the gravity field in the planetary or stellar interior is radially inwards towards the centre of mass whereas the standard gravity in the laboratory has a unidirectional and constant gravity downwards.

This paper suggests and evaluates a technique to approximate a central force field through the magnetic field from a magnet acting on a magnetic liquid using a Finite Element analysis. The model of thermomagnetic convection in a spherical shell was developed from an earlier experimental and numerical study by Früh (2005) on the control of heat transfer through a rectangular enclosure. That study demonstrated successfully that thermomagnetic convection can effectively override a gravitationally stable thermal stratification and mimic natural convection. Within the scope of this paper, only the effect of the geometry of the effective buoyancy force is considered but clearly any complete analysis will have to consider a number of other strong effects, most notably the effect of the background rotation of the system. Other important factors are, for example, differential rotation of the inner core relative to the outer shell, magnetohydrodynamics, and phase changes such as solidification resulting from the gradual cooling of the planet.

The remainder of this section gives a brief overview over previous experimental approaches to reproduce a central force field and the basic principle of thermomagnetic convection in a magnetic liquid. Section 2 describes the general modelling approach. The results from the model of convection are then described in Sect. 3, which is followed by the discussion and conclusion.

### 1.1 Experiments for convection in spherical shells and radial force fields

The traditional laboratory realisation of a central gravity field is either by a voltage difference across the spherical shell or by placing an arrangement of permanent magnets within the core of the shell. Using dielectric convection in a spherical conductor results in a highly regular central force field which decays rapidly with radius resulting in an effective gravity, $g_e \propto 1/r^5$, as stated by, e.g. Beltrame et al. (2005)[1]. As a result of this rapid decay and very high voltages required, it is relatively easy to achieve a central force field near the inner core which exceeds terrestrial gravity but not towards the outer shell. Amara and Hegseth (2002) observed a flow

*Correspondence to:* W.-G. Früh
(w.g.fruh@hw.ac.uk)

[1] Beltrame, P., Travnikov, V., Gellert, M., and Egbers, C., GEOFLOW: Simulation of convection in a spherical gap under central force field, Nonlin. Processes Geophys., submitted, 2005.

**Table 1.** Physical and nondimensional parameters of experimental sequence used for analysis.

| Geometry, temperatures, and permanent magnets | | | | Fluid properties | | | |
|---|---|---|---|---|---|---|---|
| Inner radius | $R_i$ | 35 | mm | Density | $\rho$ | 1180 | $\mathrm{kgm}^{-3}$ |
| Outer radius | $R_o$ | 100 | mm | Kinematic viscosity | $\nu$ | $1.69\times10^{-6}$ | $\mathrm{m}^2\mathrm{s}^{-1}$ |
| Domain radius | | 200 | mm | Thermal diffusivity | $\kappa$ | $0.119\times10^{-6}$ | $\mathrm{m}^2\mathrm{s}^{-1}$ |
| Mean Temperature | $T_0$ | 300 | K | Specific heat | $C_p$ | 4200 | $\mathrm{Jkg}^{-1}\mathrm{K}^{-1}$ |
| Temperature Difference | $\Delta T$ | $\pm10$ | K | Volume expansion coefficient | $\alpha_0$ | $0.18\times10^{-3}$ | $\mathrm{K}^{-1}$ |
| Magnetisation, config. B | $M_0$ | $160\times10^3$ | $\mathrm{Am}^{-1}$ | Saturation magnetisation | $M_S$ | $15.61\times10^3$ | $\mathrm{Am}^{-1}$ |
| Magnetisation, config. C | $M_0$ | $480\times10^3$ | $\mathrm{Am}^{-1}$ | Magnetic moment of ferromagnetic particles | $m$ | $2.93\times10^{-25}$ | $\mathrm{JmA}^{-1}$ |
| Nondimensional parameters | | | | | | | |
| Prandtl No. | $Pr$ | 14.2 | | Magnetic Rayleigh No., conf. B | $Ra_M$ | $5\times10^6-5\times10^8$ | |
| Rayleigh No. | $Ra_0$ | $2.41\times10^7$ | | Magnetic Rayleigh No., conf. C | $Ra_M$ | $10^7-3\times10^8$ | |

where the dielectric forces resulted in strong small-scale convection in a thin layer around the inner core of a spherical capacitor but standard convection everywhere else. To simulate a central force field everywhere in the fluid, such an experiment must be carried out in a microgravity environment, which was first carried out by Hart et al. (1986) in a hemispherical shell, and is now being prepared to operate on the International Space Station by Egbers et al. (2003). The hardware analysis is supplemented by numerical modelling by Travnikov et al. (2003) and a bifurcation analysis by Beltrame et al. (2003). Recently, Beltrame et al. (2005)[1] investigated a test of the experiment under terrestrial conditions in a numerical simulation. Again they found that the electric forces could not substantially alter the large-scale flow. However, they found that even a moderate electric force could initiate oscillatory flow.

The use of magnetic fluids for geophysical experiments was first presented by Ohlsen and Rhines (1997) for internal equatorial waves. Using a permanent magnet results in a spatially more complex field which depends in the near field on the shape of the magnet and approaches that of a dipole in the far field. Rosensweig et al. (1999) measured in their experimental set-up a magnetic field of $H_0\propto r^{-2.64}$ on the polar axis[2] and $H_0\propto r^{-3.71}$ on the equator which would lead to a very complicated gradient field, $|\nabla H|$. Their setup consisted of three stacked magnets occupying most of the core. They observed that a magnetic force could result in a longitudinal variation of the convection cells. As they used a rather thin shell, the occurrence of zonal waves is not surprising. The thin shell case of thermal convection in a non-rotating shell was recently presented by Li et al. (2005) who investigated the effects of the co-existence of many unstable modes. Unlike the experiments, which have all resulted in a radially rapidly decreasing force, Li et al. (2005) employed a linearly increasing gravitational field to model buoyancy within a fluid shell, using the Earth's mantle as an example of a moderately thin shell (with $R_i/R_o$=0.5) and Mercury's mantle as a very thin shell (with $R_i/R_o$=0.8475), compared to a radius ratio for the Earth's core of ≈0.35.

[2] Rosensweig et al. (1999) in fact quote $r^{2.64}$ but this must be a misprint.

### 1.2 Thermomagnetic convection

A magnetic liquid, also known as ferrofluid™, is a suspension of ferromagnetic nanoparticles covered with a surfactant and typically 10 nm in diameter in a carrier liquid of choice (Rosensweig, 1985, Sect. 1.3). Depending on the application the carrier liquid may, for example, be water, a hydrocarbon oil, or a silicone fluid.

Thermomagnetic convection is based on the phenomenon that a hotter magnetic fluid is less magnetised by an external magnetic field than a cooler fluid. Since the fluid experiences a force towards the magnet, cooler fluid experiences a net force towards higher magnetic fields while the warmer fluid experiences a net force away from the magnet. As such, thermomagnetic convection mimics natural convection where the magnetic field gradient is equivalent to gravity and the differential magnetisation equivalent to the thermal expansion (Rosensweig, 1985, Sect. 7.9).

The heat transfer by natural convection, caused by buoyancy of a warmer fluid underneath a cooler fluid is characterised by the Nusselt number, $Nu$, where $Nu$=1 would indicate heat transfer by conduction only, and $Nu$>1 enhanced heat transfer by convection. The force balance of buoyancy to, essentially, viscous dissipation is quantified by the Rayleigh number, Ra, such that $Nu=Nu(Pr, Ra)$, with

$$Ra = \frac{D^3\alpha_0 g\Delta T}{\nu\kappa}, \tag{1}$$

where $D$ is the reference length which is the gap width for the spherical shell. The other parameters are $\alpha_0$ the volume expansion coefficient, $g$ the gravity, $\Delta T$ the imposed temperature contrast between the boundaries, $\nu$ the kinematic viscosity, and $\kappa$ the thermal diffusivity, with values for this case as listed in Table 1.

A similar process is caused by the fact that a magnetic fluid is magnetised and thereby attracted by magnets. In other words, the fluid with a magnetisation, **M**, experiences a body force towards higher magnetic fields, of the form $\mu_0 \mathbf{M}|\nabla H|$, known as the Kelvin force. The magnetisation of magnetic fluids is usually given by a Langevin equation,

$$M = M_S \left( \coth \alpha - \frac{1}{\alpha} \right), \tag{2}$$

where $M_S$ is the fluid's saturation magnetisation and $\alpha = \frac{mH}{kT}$ with $m$ the magnetic moment of the suspended ferromagnetic particles, $H$ the imposed magnetic field, $k$ the Boltzmann constant, and $T$ the fluid's temperature. This implies that the magnetisation not only depends on the magnetic field but also the temperature. An increase in temperature results in a smaller magnetisation and thereby a smaller Kelvin force, proportional to $(\partial M/\partial T)_H$, known as the pyromagnetic coefficient. Thus, a cooler fluid is attracted to the magnet more than a warmer fluid. If the warmer fluid is near the magnet, there will be a net force for it to move away and make way for cooler fluid. As such we have a direct equivalent between this force and buoyancy if we replace gravity by the magnetic field gradient and the volume expansion coefficient by the pyromagnetic coefficient. This leads to a corresponding definition of a magnetic Rayleigh number as

$$Ra_M = \frac{D^3}{\nu\kappa} \frac{\mu_0}{\rho} \left( \frac{\partial M}{\partial T} \right)_H |\nabla H| \Delta T. \tag{3}$$

## 2 Description of models

### 2.1 The physical system

The physical system studied here attempts to model a small-scale laboratory based experiment of convection in the Earth's core. A diameter of 200 mm of the sphere containing the fluid was chosen. This size is somewhat larger than that by Rosensweig et al. (1999) and by Beltrame et al. (2005)[1] and much larger than the original Spacelab experiment by Hart et al. (1986). A radius ratio of $R_i/R_o$=0.35 resulted in an inner radius of the fluid shell of $R_i$=35 mm. At this stage of the study, only convection in a stationary fluid cell was considered, and the other essential features of the rapid background rotation and differential shear between the inner core and mantle will be the focus of a follow-on study. The only laboratory experiments carried out to date in terrestrial gravity conditions, by Amara and Hegseth (2002) and Rosensweig et al. (1999), have not considered a rotating shell either and provide a useful comparison to the results presented here.

All laboratory experiments so far have only considered a rapidly decaying central force field. In the case of using a spherical capacitor and an electrophoretic fluid, an effective gravity field of $g_e \propto r^{-5}$ is a necessary consequence of the experimental design, e.g. Amara and Hegseth (2002). Rosensweig et al. (1999) generated a similar force field by placing an arrangement of permanent magnets in the core of the system. While gravity outside a body of mass does decay with $g \propto r^{-2}$, it increases linearly within that body (Li et al., 2005). This paper considers both cases by using different arrangements of magnets as described in Sect. 2.2.

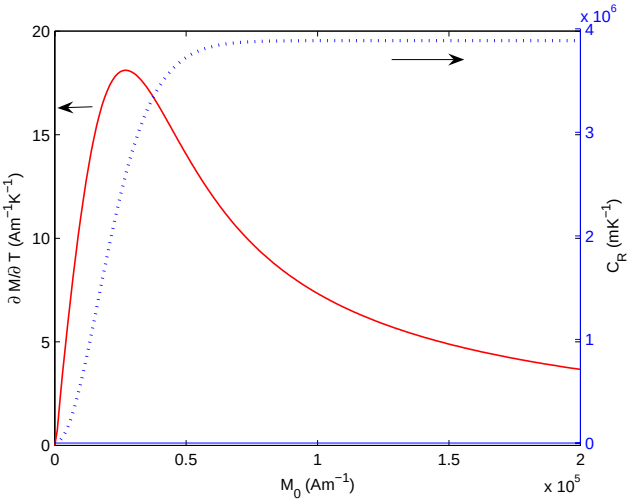


**Fig. 1.** Variation of the pyromagnetic coefficient, $(\partial M/\partial T)_H$ (red solid line, left axis), as a function of the magnetic field, $H$, at a reference temperature of $T$=300 K, and the scaling of the magnetic Rayleigh number with the strength of the magnets, $C_R$ (blue dotted line, right axis).

Since the proposed experiment was inspired by an experiment on thermomagnetic convection in a rectangular box by Früh (2005), the same fluid properties of the water-based Ferrotec™ EMG805 300 Gauss magnetic fluid and the specification of existing magnets were chosen for the initial analysis and are listed in Table 1. Using a temperature contrast across the shell of $\Delta T$=10 K, the system is characterised by a standard Rayleigh number of $Ra$=2.4×10$^7$ which is only a little smaller than the estimate of $Ra \sim O(10^8)$ by Rosensweig et al. (1999) for convection in the Earth's mantle but is much smaller than that for the Earth's core, estimated by Gubbins (2001) to be in excess of $10^{12}$, or even $Ra > 10^{20}$ as stated by Aurnou et al. (2003).

To estimate the magnetic Rayleigh numbers anticipated in the experiment, an analysis of the Rayleigh numbers achieved by the chosen magnetic fluid and magnets was carried out using the strength of the magnets, $M_0$, as a control parameter, which affects both the pyromagnetic coefficient, $\partial M/\partial T$, and the field gradient, $|\nabla H|$. Varying the magnets' strength but maintaining their size and arrangement, the field gradient scales linearly with $M_0$, whereas the pyromagnetic coefficient, obtained by differentiating Eq. (2) with respect to temperature, depends on the local magnetic field as shown by the solid line in Fig. 1 with a rapid increase to a maximum of about 18 Am$^{-1}$K$^{-1}$ near a local field strength of about 20 kAm$^{-1}$, followed by a decrease which is asymptotically $\propto H^{-1}$. Since the magnetic Rayleigh number is proportional to both, the pyromagnetic coefficient and the field gradient, the dotted line in Fig. 1 shows the

quantity $C_R=D^3\mu_0/(\nu\kappa\rho)\times(\partial M/\partial T)\times M_0$, taking into account all factors in Eq. (3) except the temperature contrast and the normalised field gradient, $Ra_M=C_R|\nabla(H/M_0)|\Delta T$. As the dotted line shows, this factor increases rapidly until about 40 $\mathrm{kAm}^{-1}$ and then levels off at a value of about $3.9\times10^6$ $\mathrm{mK}^{-1}$. For a typical dipole field of a magnet of size 30 mm with unit magnetisation, the gradient is $O(100\ \mathrm{Am}^{-2})$ near the magnet and $O(1\ \mathrm{Am}^{-2})$ at a distance of about 100 mm. With a temperature contrast of $\Delta T=10$ K, we could therefore expect a magnetic Rayleigh number in the range of $Ra_M\approx10^7-10^9$ in the fluid domain.

### 2.2 Model formulation

Since this study was a proof-of-concept investigation rather than an accurate prediction of flow fields in such a laboratory experiment, it was decided to consider only the axisymmetric case of a 2D section through the shell. While it is expected that the three-dimensional flow will differ from the two-dimensional results, the force balance between gravity and the Kelvin force would not be affected by this simplification. Only with this simplified 2D approach was it possible to explore the range of configurations presented here which can be taken as a guide for further three-dimensional calculations.

The numerical model was a 2D Finite-Element model which was developed using the package FEMLAB™. Since this package is a very flexible tool in which different physical systems can be coupled, the model included the field equations for the magnetic field as well as the conduction-convection equation for the temperature and the Navier-Stokes equations for the fluid velocities. Unlike all previous studies, we could therefore calculate the actual magnetic field from the permanent magnet, and the resulting magnetisation of the magnetic fluid, rather than imposing an arbitrary or analytical field. The Kelvin force was then found by calculating the pyromagnetic coefficient from an analytical differentiation of the Langevin equation, Eq. (2), and the local values of the magnetic field and the fluid temperature, and by calculating the local gradient of the magnetic field, $\nabla|H|$.

Three types of convection were investigated; first, free convection under specified central gravity fields, and then two configurations of thermomagnetic convection with and without natural convection under vertical gravity of a terrestrial laboratory environment.

All cases consisted of a fluid domain in a spherical shell with an inner radius of $R_i=35$ mm and an outer radius of $R_o=100$ mm, where no-slip boundary conditions were applied to both boundaries and a zero pressure reference to the left-most point on the outer boundary. Surrounding the outer perspex shell of the modelled apparatus was a further shell of radius 200 mm which was included in the magnetic field calculations only.

The magnetic field equations were solved using the magnetic vector potential, $\mathbf{A}=(0,\,0,\,A_z)$, from which the horizontal magnetic field is found by $\mathbf{B}=\nabla\times\mathbf{A}$ or $B_x=\partial A_z/\partial y$ and $B_y=-\partial A_z/\partial x$:

$$\frac{1}{\mu_0\mu_r}\nabla\times\nabla\times A_z=0 \tag{4}$$

with $\mathbf{B}=\mu_0\mu_r\mathbf{H}$ everywhere except in the magnet and the magnetic fluid, where $\mu_r$ is the relative permeability of the material, metal for the inner core ($\mu_r=1.3$), perspex for the outer shell ($\mu_r=0.9998$), and air for the surrounding space ($\mu_r=1$). The magnet and the magnetic fluid used

$$\nabla\times\left(\frac{1}{\mu_0}\nabla\times A_z-\mathbf{M}\right)=0 \tag{5}$$

with $\mathbf{B}=\mu_0(\mathbf{H}+\mathbf{M})$, where the magnetisation of the magnet was given as $\mathbf{M}=(0,\,M_0)$ (or rotated by an appropriate angle for configuration C), and the magnetisation of the fluid was calculated using Eq. (2). Assuming the external boundary of the whole domain was sufficiently far away from the magnet, Dirichlet boundary conditions of $A_z=0$ could be applied.

The continuity and momentum equations were

$$\nabla\cdot\mathbf{u}=0 \tag{6}$$

and

$$\rho\frac{\partial\mathbf{u}}{\partial t}+\rho\,(\mathbf{u}\cdot\nabla)\,\mathbf{u}=\nabla\left(p\mathbf{I}+\eta\left[\nabla\mathbf{u}+(\nabla\mathbf{u})^T\right]\right)+\mathbf{F} \tag{7}$$

with $\eta$ the dynamic viscosity. The force term $\mathbf{F}$ could represent either the Kelvin force,

$$\mathbf{F}_K=\mu_0\left(\frac{\partial M}{\partial T}\right)_H\nabla|H|(T-T_0), \tag{8}$$

with or without the buoyancy,

$$\mathbf{F}_b=\rho g\alpha_0\,(T-T_0)\,\mathbf{e}_y, \tag{9}$$

added to it, or the central force field,

$$\mathbf{F}_c=\rho g\alpha_0\,(T-T_0)\left[\left(x^2+y^2\right)/R_o^2\right]^{n/2}\mathbf{e}_r, \tag{10}$$

where $n$ is the scaling of the central force field, The factor $R_o$ ensured that the local gravity at the outer boundary was equal to the terrestrial gravity, $g=g_0\equiv9.81\ \mathrm{ms}^{-2}$. The boundary conditions were no-slip conditions on both boundaries, together with a zero pressure reference at one point on the outer boundary.

The heat equation, solving for the temperature, $T$,

$$\frac{\partial T}{\partial t}+(\mathbf{u}\cdot\nabla)T=\kappa\nabla^2T \tag{11}$$

was applied to the fluid part of the domain only, with Dirichlet boundary conditions, $T_i=T_0+\Delta T/2$ and $T_o=T_0-\Delta T/2$ at the inner and outer boundary, respectively.

*Configuration A*, which addressed free convection only, solved the Navier-Stokes equations and the heat conduction and convection equation in the fluid domain. The driving force was a central buoyancy force, Eq. (10) with $n=-5,\,-4,\,\ldots\,5$. The case of $n=-2$ corresponds to gravity

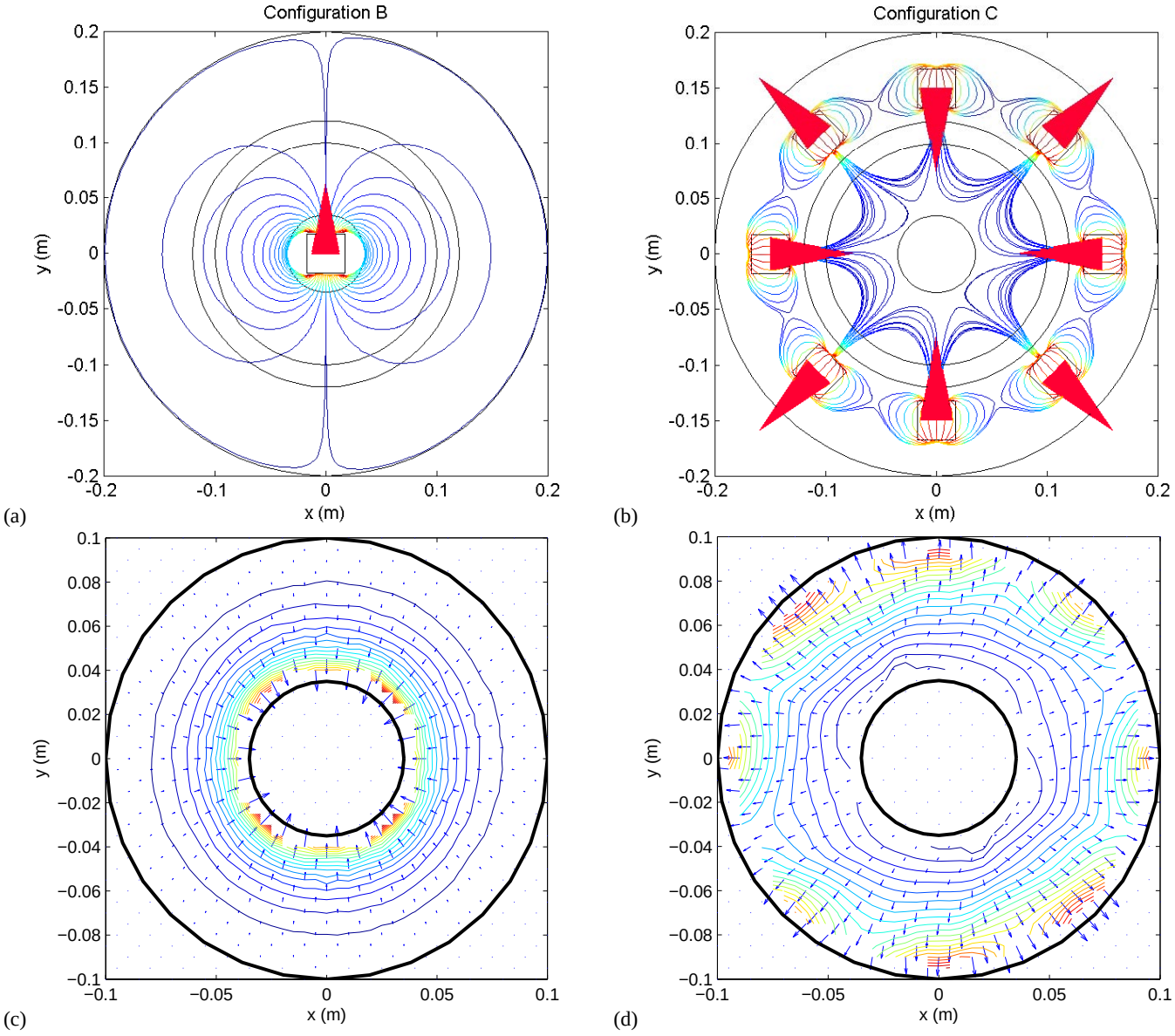


**Fig. 2.** The magnitude and direction of the magnetic field and its gradient for either configuration B (**(a)** and **(c)**) or configuration C (**(b)** and **(d)**). (a), (b) Field lines of the magnetic field **H** together with the direction of the magnetisation of the subdomains representing the permanent magnets, shown by the cones placed at the centre of each magnet. (c), (d) Contour lines of the magnitude of $\nabla|H|$, with blue indicating a weak gradient and red a strong gradient, and arrows of the gradient field.

outside a body whereas $n = 1$ corresponds to gravity within the body.

To form the second system, *configuration B*, a single permanent magnet of square cross-section, with an edge length of 35 mm and a magnetisation of 160 kAm$^{-1}$ in the vertical, was placed in the centre of the core. The full domain for configuration B had a radius of 200 mm to solve the magnetic field equations with magnetic insulation at the outer boundary. The conduction-convection equation and the Navier-Stokes equations were solved only in the sub-domain of the magnetic fluid, and the force to drive thermomagnetic convection was the Kelvin force, Eq. (8), which was applied in isolation as well as added to the buoyancy in a terrestrial laboratory, Eq. (9).

Since the thermomagnetic convection in a laboratory is the focus of this paper, the full thermomagnetic and natural convection in configuration B was taken as the benchmark for all other results. To start from identical, non-trivial initial conditions, the following procedure was followed. Initially, the magnetic field for configuration B was solved by a linear solver independent of the momentum and heat equations. The field in the fluid domain was solved for **M** at the reference temperature $T_0$. This was possible since the changes of the fluid's magnetisation with temperatures would only have a negligible effect on the overall magnetic field. The result for the magnetic field due to the uniform magnetisation of the magnet at the core is shown in Fig. 2a.

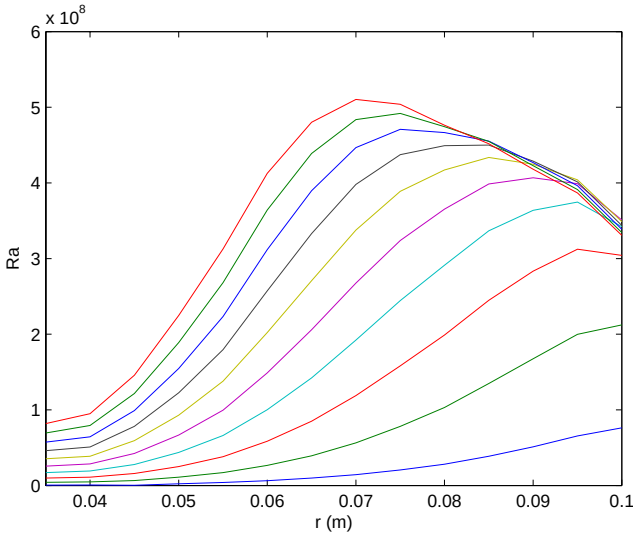


**Fig. 3.** Radial variation of the local Rayleigh number, azimuthally averaged for a range of magnetisation strengths of the magnets surrounding the shell. The lowest line shows magnets with $M_0$=160 kAm$^{-1}$ (same as for configuration B), the top line with $M_0$=1600 kAm$^{-1}$. The spacing between the curves are 160kAm$^{-1}$.

Once the magnetic field and the fluid's magnetisation were calculated. A relatively coarse resolution time marching integration of the momentum and heat equations incorporating both, Eq. (8) and standard buoyancy, was performed. The spatial structure of the field gradient used in Eq. (8), shown in Fig. 2b appears sufficiently symmetric to result in a central force field, decaying with distance from the core. A regression of the magnetic field gradient to a power-law dependence on $r$ resulted in $|\nabla H|=(200\pm20)r^{-3.0\pm0.05}$ where the 'uncertainty' in the proportionality constant largely reflects deviations from rotational symmetry. After a time of 500 s, the solution appeared to have settled. To test whether the initial resolution of 972 elements was adequate, the resolution in the fluid domain was increased such that the full domain of configuration A and B contained 2050 elements. While this resulted in a somewhat higher rate of heat transfer, the flow field itself was not substantially changed. The adjustment to the higher resolution was achieved within the first few seconds of the integrations, and it was deemed adequate to use the final time step of the lower resolution spin-up run as the initial condition for all further integrations presented here.

To define the final system, *configuration C*, a set of eight magnets of the same size as that used in configuration B were placed in the outermost shell of the domain, equally distributed in azimuth and with a distance from the centre of 150 mm. They were orientated such that pole faces of alternating polarity pointed to the centre of the domain, as indicated by the cones in Fig. 2b. Configuration C had 3582 elements due to the higher number of subdomains representing the eight magnets while keeping the resolution in the fluid domain similar to that of configuration B. To achieve a magnetic field strong enough to overcome gravity within the fluid domain, the magnetisation of the magnets was increased by a factor of 3 as justified in Sect. 2.3. Since the Kelvin force now is directed radially outwards rather than inwards, the temperature contrast was inverted; the surface at the inner core was held at a cooler temperature while the outer surface was heated. To give a comparable visual impression of the temperature field, the results for these configurations show $-T$ so that the temperatures near the core are displayed in warm colours and the temperatures near the outer surface in cool colours, respectively.

### 2.3 The Rayleigh numbers

Since the local strength of gravity or the Kelvin force varies, the local Rayleigh number also varies. Using the standard definition of the Rayleigh number, Eq. (1), but varying $g$ with radius for the different force fields, one can compute effectively a local Rayleigh number and compare this to the local magnetic Rayleigh number.

Based on the analysis of the pyromagnetic coefficient and the scaling factor for the magnetic Rayleigh number, both shown in Fig. 1, a range of specifications for the magnets in configuration C was analyzed. Figure 3 shows the radial variation of the magnetic Rayleigh number for magnets with a magnetisation ranging from 160 kAm$^{-1}$ (as used in configuration B) to 1600 kAm$^{-1}$. The progression of the lines shows that the magnetic Rayleigh number, or the Kelvin force, first increases rapidly with the strength of the magnetic field but that this increase becomes less and less for higher fields until saturation sets in. Due to the spatial variation of the gradient field, the Rayleigh number for a fluid magnetised to its saturation level reaches a peak within the fluid interior. To maintain a sufficiently strong but largely radially increasing force field, magnets with a magnetisation of 480kAm$^{-1}$ were chosen for the main analysis of configuration C.

The radial variation of the Rayleigh numbers for all configurations is shown in Fig. 4, where the thick lines represent the magnetic Rayleigh numbers and the thin lines some of the simple central "gravity" fields. The horizontal line for $g=C\mathbf{e}_r$, at $Ra=2.4\times10^7$, shows also the Rayleigh number for natural convection in the shell under "normal" gravity. The two solid lines show the realistic cases of gravity increasing linearly within a mass and decreasing quadratically outside the mass while the dotted and dashed lines are simple central force fields with similar scaling as the observed magnetic configurations. The magnetic Rayleigh number for configuration B exceeds standard gravity by a factor of 20 near the core but falls below it beyond a radius of about 70 mm, and has reduced to about 20% of standard gravity at the outer boundary. While the field magnetic field gradient decayed $\propto r^{-3}$, the magnetic Rayleigh number followed a decay $\propto r^{-5}$ very closely. This in fact is virtually identical to that of the electrophoretic convection in spherical capacitors but easily exceeds its strength. Configuration C, by virtue of using the stronger magnets, exceeds gravity beyond a radius of about 50 mm and rapidly increases to a strength of $10g_0$

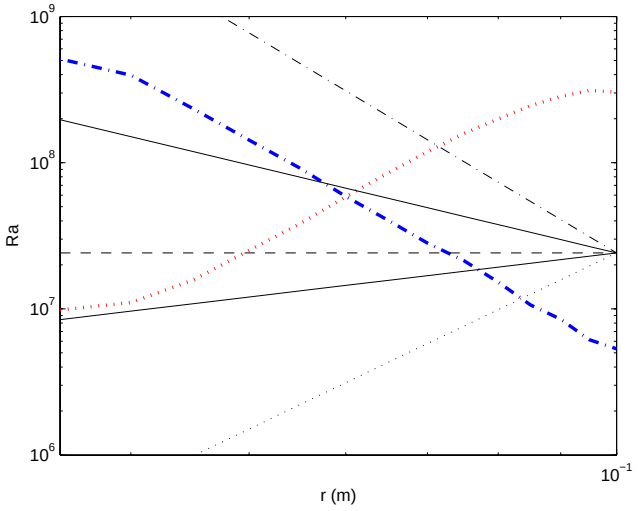


**Fig. 4.** Radial variation of the local Rayleigh number, azimuthally averaged. The magnetic Rayleigh numbers are shown as the thick lines for configuration B (dash-dotted, blue) and configuration C (dotted, red). The reference cases of central force fields $\propto r^n$ are $n$=4 (dotted), $n$=1 (solid), $n$=0 (dashed), −2 (solid), and −5 (dash-dotted).

at the outer boundary. The radial variation of this force field is consistent with a scaling $\propto r^{4.3}$.

For the purpose of defining a global characteristic Rayleigh number for each case, the local Rayleigh number at mid-radius, $r=R_i+(R_o-R_i)/2$=67.5 mm was chosen. This choice is somewhat arbitrary but was found to give a useful measure of the overall behaviour for an approximate quantitative cross-comparison of the different configurations.

## 3 Convection in a spherical shell

Since the aim of the paper was to explore configurations of thermomagnetic convection to mimic central force fields in a laboratory experiment, the majority of simulations were carried out at a fixed temperature difference. For selected configurations only, a parametric study of the effect of the temperature difference was carried out. As a result, this section describes only the results for the fixed temperature difference, while the effect of varying $\Delta T$ is only mentioned in Sect. 4.

The simulations are divided into three parts, first the free convection under a range of basic radial force fields will be presented, before thermomagnetic convection with the magnet at the core is discussed in Sect. 3.2. The final sub-section will then cover thermomagnetic convection where the magnets surround the shell. The cases presented, and their respective Rayleigh numbers, are listed in Table 2.

### 3.1 Configuration A

As benchmarks for the simulation of thermomagnetic convection, a range of central force fields of the form $\mathbf{g}=C\mathbf{r}^n$ was investigated where $n$ ranged from $n$=5 to $n$=−5, close to the force field generated by our first configuration with the magnet in the core. The constant of proportionality, $C$, was chosen such that all cases had a magnitude of $g$=9.81 m s$^{-2}$ at $r=R_o$, the outer boundary of the shell. The temperature and vorticity fields at the final iteration step for the three cases of $n$=−5, 1, 5 are shown in Fig. 5a–c, respectively, where the case $n$=1 represents the gravity field in the Earth's interior. All cases showed the same qualitative behaviour of two warm currents flowing outward from the core and two cool currents flowing inward from the outer boundary resulting in four convection cells with alternating circulation. However, a clear quantitative progression is observed from very slow and broad currents at the radially increasing "gravity" to very narrow jets and very strong convection at the rapidly decaying "gravity". As the force field is rotationally symmetric, there was no preferred position for the hot jets. During the equilibration period, the initial flow with no clear symmetry settled into the symmetric pattern of opposite jets, after which there was no noticeable rotational drift of that pattern.

**Table 2.** Configurations tested at a temperature difference of $\Delta T$ = 10K.

| Configuration | Rayleigh No | Comments |
|---|---|---|
| A, $n$=−5 | $1.721\times10^8$ | closest to configuration B |
| A, $n$=−4 | $1.162\times10^8$ | |
| A, $n$=−3 | $7.84\times10^7$ | |
| A, $n$=−2 | $5.29\times10^7$ | outside massive body |
| A, $n$=−1 | $3.57\times10^7$ | |
| A, $n$=0 | $2.41\times10^7$ | constant $g$ |
| A, $n$=1 | $1.628\times10^7$ | Earth's/ planetary/ stellar interior |
| A, $n$=2 | $1.099\times10^7$ | |
| A, $n$=3 | $7.42\times10^6$ | |
| A, $n$=4 | $5.01\times10^6$ | |
| A, $n$=4.3 | $4.45\times10^6$ | closest to configuration C |
| A, $n$=5 | $3.38\times10^6$ | |
| B | $7.18\times10^7$ | magnet in core |
| C | $7.56\times10^7$ | magnets surrounding, $\Delta T$=−10K |

The temporal behaviour of the overall heat transfer, shown by the Nusselt number in Fig. 6, suggested an equilibration towards a steady solution but attempts to calculate steady state solutions failed to converge except for some spurious cases at the lower resolution. As soon as the resolution was increased, that steady solution disappeared again. Fluctuations of the solution not clearly represented by the Nusselt number appeared to be small but persistent fluctuations of the position of the hot jets near the inner surface. As gravity became stronger and stronger near the hot core, the intensity of the convection increased, the jets became narrower, and the Nusselt number increased.

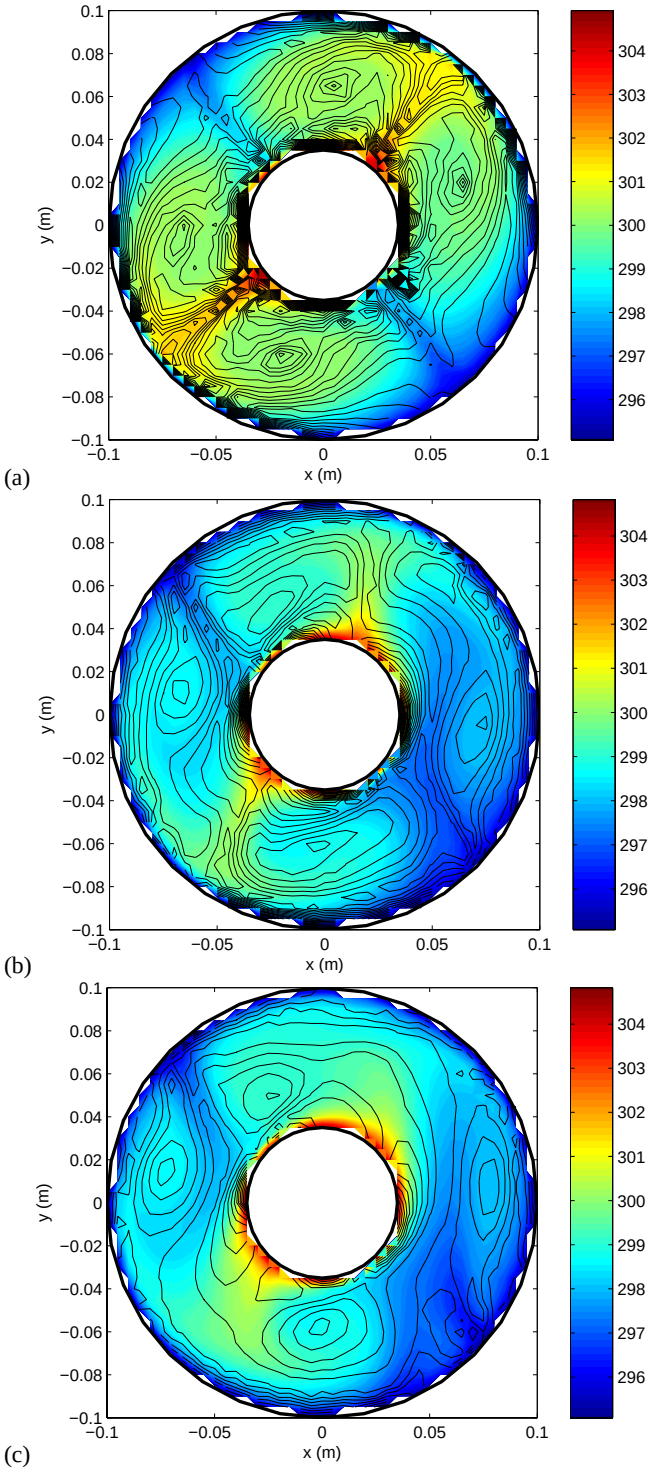


**Fig. 5.** Snapshot of the solution after 100 s of natural convection under different radial gravity fields, **(a)** $g \propto r^{-5}$, **(b)** $g \propto r$, and **(c)** $g \propto r^5$, respectively. The shaded surface shows the temperature and the contour lines the vorticity with a contour spacing of 0.1 $s^{-1}$ for (a) and of 0.025 $s^{-1}$ for (b) and (c).

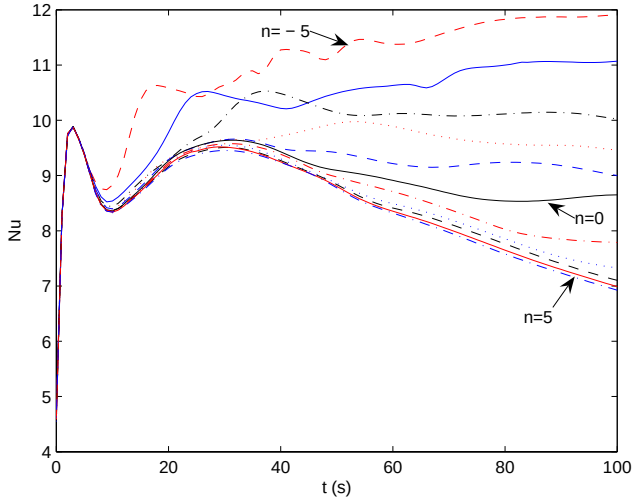


**Fig. 6.** The Nusselt number as a function of time for all radial force fields, $f \propto r^n$ with $n$ ranging from $n$=−5 to $n$=5 in integer steps. The two extreme cases and $n$=0 are labelled, and the intermediate values of $n$ form a monotonous sequence with a smaller exponent leading to a higher Nusselt number.

### 3.2 Configuration B

This section presents the full simulation of a laboratory-based experiment which combines thermomagnetic convection caused by the magnet at the core with natural convection due to standard gravity of the terrestrial laboratory environment. As presented in Sect. 2.3, the magnetic force decayed $\propto r^{-5}$ with a strength of about 20% of the central "gravity" with $n$=−5 presented in Sect. 3.1.

The simulation of thermomagnetic convection in a terrestrial laboratory, of which three time steps at $t$=80, 90, 100 s are shown in Fig. 7, shows a much more complicated flow structure than the convection in central force fields. The flow tended to be organised into three hot jets originating from the inner core, of which one jet tended to be fairly narrow and similar to those found above and two weaker and broader jets which also showed more temporal variation. A much longer integration of configuration B with gravity, for a total of 1000 s showed that the flow settled into a regular oscillation as shown by the time series of the Nusselt number in Fig. 8. While not limited to that area, the area underneath the core, where buoyancy and Kelvin force oppose each other, tended to show the greatest variability, with jets erupting and then being deflected. A typical velocity in a hot jet was about $U$=0.02 $ms^{-1}$, with a maximum of about 0.03 $ms^{-1}$.

Investigating the sensitivity of the solutions to the presence of the vertical buoyancy, an experiment was carried out in which only the Kelvin force was present. This, in effect, was a simulation of such an experiment in a microgravity environment. Without gravity, the solution, in Fig. 9, became very similar to those of the ideal central force fields, both in global appearance and temporal behaviour. The strength of the convection, as measured by the vorticity was most similar

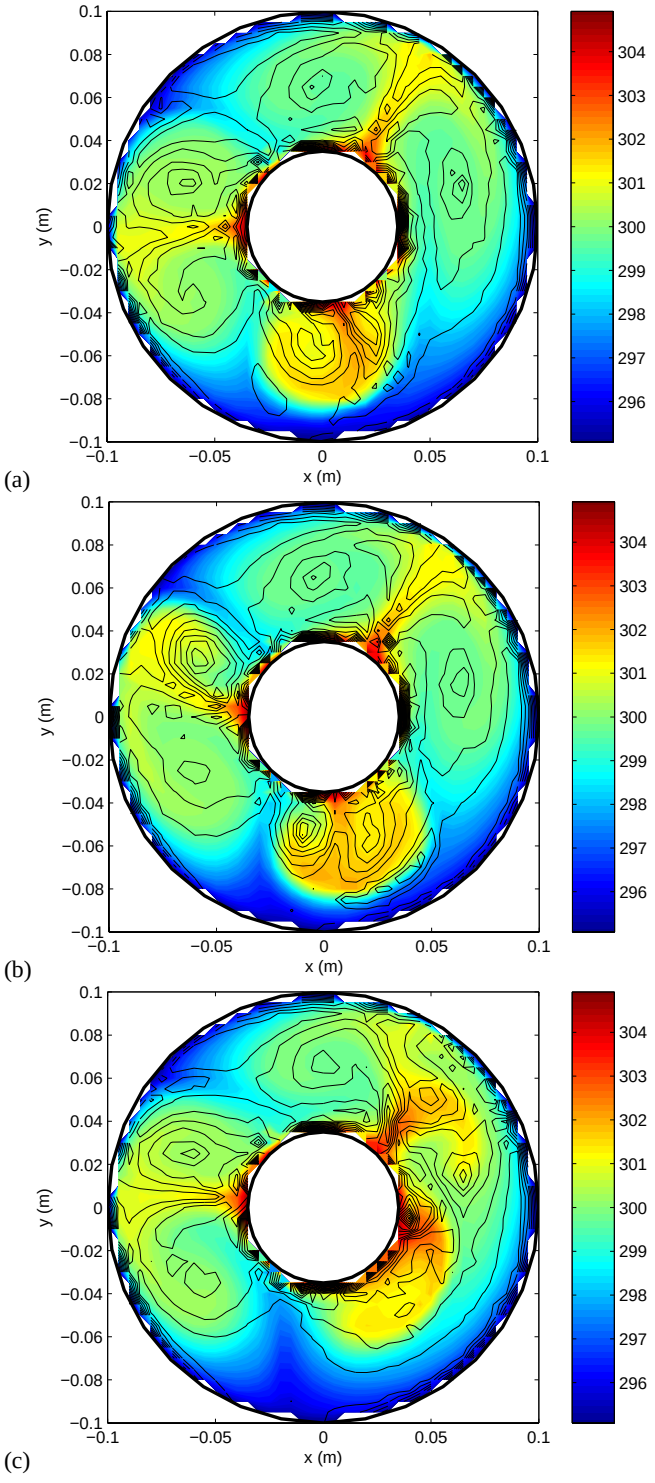


**Fig. 7.** Snapshots of the solution at 80, 90, and 100 s of thermomagnetic convection with vertical gravity of configuration B. The shaded surface shows the temperature, and the contour lines the vorticity with a contour spacing of 0.5 $s^{-1}$.

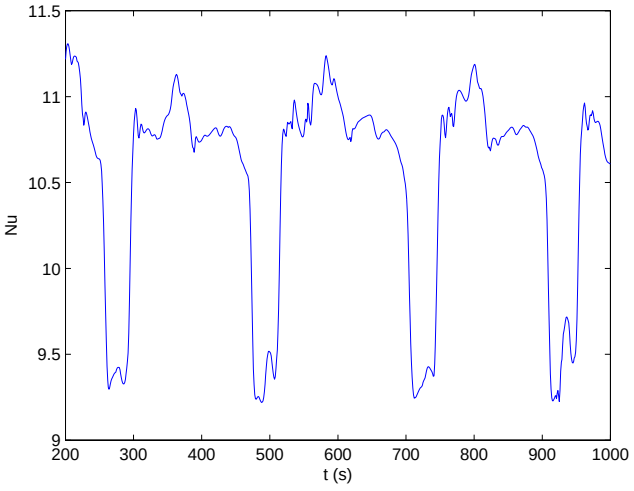


**Fig. 8.** Time series of the Nusselt number of thermomagnetic convection with gravity of configuration B.

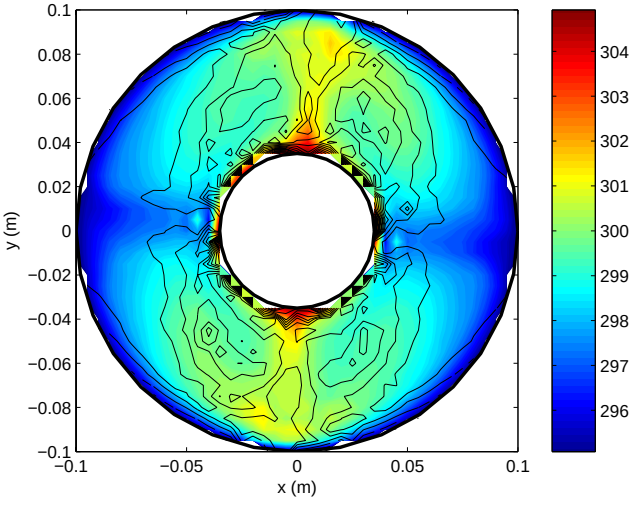


**Fig. 9.** Snapshot of the solution after 100 s of thermomagnetic convection only of configuration B. The shaded surface shows the temperature, and the contour lines the vorticity with a contour spacing of 0.5 $s^{-1}$.

to that with the similar central force field of the form $r^{-5}$, Fig. 5a. The only qualitative difference was that the convection under the Kelvin force showed a clear alignment of the hot jets with the axis of the magnetic dipole. Two separate integrations, one from the common initial condition, and one continuing from the higher-resolution case at $t$=100 s (Fig. 7c) showed the same behaviour of the jet in the upper right quadrant rapidly moving counter-clock wise, overshooting the vertical line, and then returning to a vertical position.

A final control experiment of vertical gravity only, confirmed the expected convection pattern of a single hot plume rising from the top of the core and setting up a large-scale return circulation in two left-right symmetric overturning cells.

The fact that the two separate cases appeared to converge to (almost) steady solutions but that the full model did not was not surprising as there will be a spatially varying competition between buoyancy and the Kelvin force, both in strength and direction. The Kelvin force is much stronger

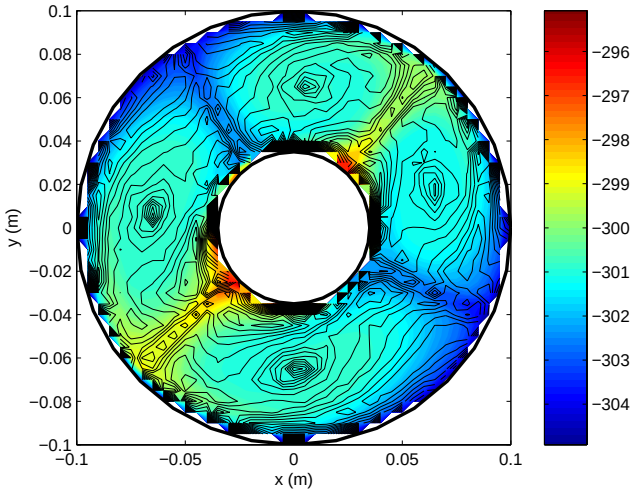


**Fig. 10.** Snapshot of the solution after 100 s of thermomagnetic and natural convection of configuration C. The shaded surface shows the temperature and the contour lines the vorticity with a contour spacing of 0.5 $s^{-1}$.

than buoyancy near the core but much weaker near the outer boundary, and the direction of the Kelvin force is largely towards the core while the buoyancy is vertical. Both factors together lead to a complex pattern of the effective body force on the fluid which provides an intuitive explanation, for example, why the plume downwards from the bottom of the core tended to be the weakest and shortest plume and why it tended to be diverted into an upward direction once it extended somewhat into the fluid interior. While it provides an explanation as to why an upward jet should be the most intense, the superposition of the Kelvin force and buoyancy does not give an immediately obvious explanation for the observation that this jet is not from the top of the core but at an angle, whereas the two forces separately showed a clear preference for a vertical plume rising from the top of the core. The reason for this is as yet not understood.

### 3.3 Configuration C

This section presents the alternative laboratory-based experiment of thermomagnetic convection caused by magnets surrounding the shell. Using the somewhat stronger magnets, the magnetic forces in this configuration resulted in a radially increasing force equivalent to a central force field of $g_e$=$20g_0(r/R_o)^{4.3}$ with an effective "gravitational" acceleration of $20g_0$ at the outer boundary, as shown in Sect. 2.3.

The convection caused by this radially increasing magnetic field is shown in Fig. 10. As mentioned in the methodology, the temperature contrast is inverted, since the Kelvin force has an outward direction, resulting effectively in an inward buoyancy. This flow is closer to the ideal cases of the central force fields described in Sect. 3.1 in that it settled in a solution with two jets emerging from the inner core and two return jets from the outer boundary, resulting in four convection cells but there are some differences. The jets from the thermomagnetic convection are much stronger, and the convection cells are less symmetric. The solution shows a pair of large cells and a pair of smaller cells. As with the other configuration, the solution showed substantial persisting temporal fluctuations.

As with the thermomagnetic convection of configuration B, the superposition of buoyancy–which would result in a single upward plume of warm fluid from the bottom–and the Kelvin force, does not show the expected up-down preference seen in the convection caused by the forces separately. The simulation of this thermomagnetic convection without gravity resulted in a flow pattern very similar to that of the full case.

A test case using weaker magnets with $M_0$=160 $kAm^{-1}$, resulted in a flow very similar to that of natural convection only. The other extreme case of strong magnets with $M_0$=1600 $kAm^{-1}$ magnetisation showed very similar behaviour to that shown in Fig. 10 for the intermediate magnets. The heat transfer with the strong magnets was even a little below that found for the intermediate case. Früh (2005) demonstrated that a competition between buoyancy and Kelvin force resulted in a competition where both forces seemed to contribute only over a fairly small range of relative magnitude; once one of the two forces was about twice the other, the flow was largely dominated by that force only. Since the Kelvin force with the weaker magnets was noticeably larger than buoyancy near the outer surface but much smaller near the core, it appears that the relative strength of the two forces near the core determines whether natural convection or thermomagnetic convection is seen. A full parametric investigation, however, is required to confirm this indication.

## 4 Discussion of results

Both magnetic configurations resulted in substantial thermomagnetic convection. Both, the flow field pattern and its temporal evolution, in configuration C were very similar to those observed in the simple central force fields. Configuration B, on the other hand, showed more differences in the structure of the flow and persistent, stronger variability. Fig. 11 shows the temporal evolution of the Nusselt number for thermomagnetic convection with gravity for configuration B (thick solid line) and configuration C (thick dotted line), thermomagnetic convection without gravity (thin solid and dotted lines, respectively), and the two central force fields following the magnetic forces most closely, $g$=$0.2g_0(r/R_0)^{-5}$ for configuration B (dashed line), and $g$=$20g_0(r/R_0)^{4.3}$ for configuration C (dash-dotted line), respectively.

The difference between the presence and absence of gravity in configuration C was very small (the two dotted lines in Fig. 11), and it appears that terrestrial gravity at the chosen strength of magnets had no significant effect on the convection, even though gravity was stronger by a factor of about 2, cf. Fig. 4, at the core. The corresponding central "gravity" resulted in a much smaller heat transfer (the dash-dotted

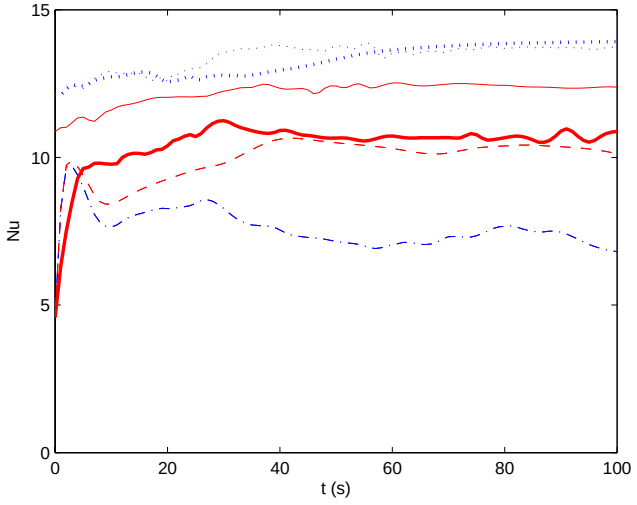


**Fig. 11.** The Nusselt number as a function of time for the two magnetic configurations. Red lines correspond to the radially decreasing fields (B and A with $n$=−5) while blue lines show the radially increasing fields (C and A with $n$=4.3) . The solid lines show the Nusselt number for configuration B with the magnet at the core, where the thin line is the thermomagnetic convection by the Kelvin force alone while the thick line is the convection caused by the Kelvin force and laboratory gravity combined. The dotted lines are the corresponding cases for configuration C, with the magnets surrounding the shell. Two reference cases of a central field decaying $\propto r^{-5}$ (dashed line) and a force field increasing $\propto r^{4.3}$ (dash-dotted line) are shown for comparison.

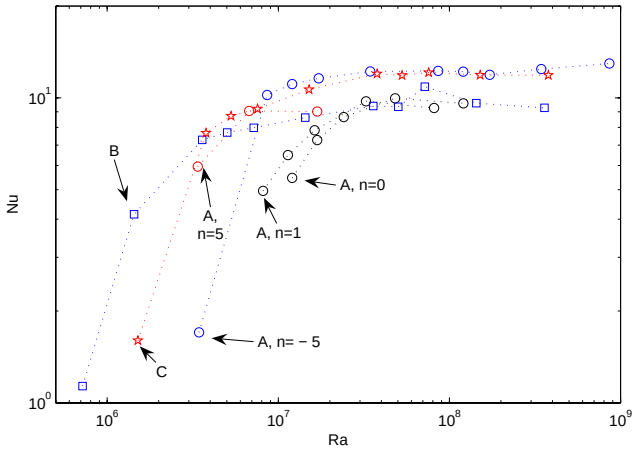


**Fig. 12.** The Nusselt number for selected configurations A with $n$=−5, 0, 1, and 5, and for configurations B and C (both with terrestrial gravity), and against the reference Rayleigh number.

line). Even though the strength of the central field was increased by a factor of 20 compared to the cases of configuration A presented in Sect. 3.1, the Nusselt number was very close to those found for the cases with $n$=4 and 5. While the central force fields had the symmetry that the imposed temperature gradient was aligned with the gravity, the spatial structure of the magnetic field, especially its azimuthal variation, resulted in components of the Kelvin force off the radial direction. Früh (2005) suggested that a spatial variation of the Kelvin force, which may have a component perpendicular to the imposed temperature gradient, could result in enhanced convection, rather like the superposition of a fluid heated from below and from the side.

Configuration B was more susceptible to the presence or absence of gravity. This may be due to the magnetic forces being smaller than gravity over a sizeable part of the domain. Gravity exceeded the magnetic forces by a factor of 5 at the outer boundary. In the absence of gravity, both, the flow pattern and its time dependence, were qualitatively the same as that of the central force fields. While the zero-gravity case appeared to settle into an almost steady state, the terrestrial laboratory case showed persistent fluctuations, as demonstrated by the two solid lines in Fig. 11. The presence of gravity somewhat reduced the heat transfer, presumably because the hot jets could not extend to the outer boundary without being deflected. The quantitative agreement between configuration B and the central force field (the dashed line) was much closer but the cases with the more similar force fields showed the same qualitative difference as for configuration C; configuration B without gravity showed a higher rate of heat transfer than the central force field. As with configuration C, the heat transfer enhancement may have been caused by azimuthal variations of the magnetic field and a resulting spatial variation of both, the strength and direction, of the driving force. Since the deviation from azimuthal symmetry of the magnetic field for configuration B was much smaller than that for configuration C, as demonstrated in Figure 2c and d, it is not surprising that the difference in the Nusselt number between configuration B without gravity and the central force field was much less than for the other configuration. The larger difference between configuration B with and without gravity can be explained by the facts that the magnetic force was, on average, not as large as that for the other configuration and that its azimuthal variation is much smaller. As a result, adding gravity will have a much stronger effect on the strength and direction of the overall body force.

The behaviour of the convection on changing the temperature contrast between the boundaries was tested for a few selected configurations, namely the full thermomagnetic convection cases with added terrestrial gravity, B and C, and the central force fields, configuration A, with $n$=−5, 0, 1, and 5. Temperature differences ranging from $\Delta T$=0.1 K to 50 K were tested, where the final solution at $\Delta T$=10 K was the initial condition for the next higher and next lower temperature difference. For each successively increased or decreased temperature difference, the integration was then continued from the last integration. The Nusselt number at the end of each integration is shown against the reference Rayleigh number in Fig. 12. The onset of convection above a critical Rayleigh number can be seen clearly after which the Nusselt number rapidly increases to $Nu$=$O$(10). On further increase of the temperature difference, the Nusselt number varies only slightly. Since the reference Rayleigh number was determined in a somewhat ad-hoc fashion as that at mid-radius,

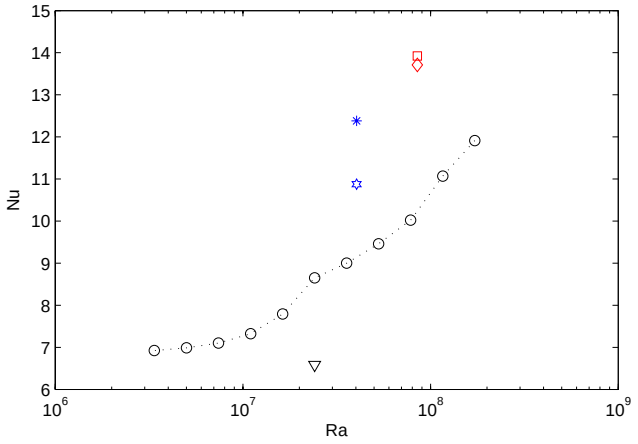


**Fig. 13.** The Nusselt number at the end of the integrations for all types of convection discussed here. The x-axis is the reference Rayleigh number of each case. The open circles joined by the dotted line are the results from configuration A of central force fields. The black triangle: Natural convection under vertical gravity. Blue symbols for radially decreasing field, B: six-pointed star for thermomagnetic convection with gravity and "$*$" without gravity. Red symbols for the radially increasing field: the square is for thermomagnetic convection with gravity, the diamond without.

the fact that the convection sets in at different critical values should not be over-interpreted. However, one has to bear in mind that there is no immediate reason why the critical Rayleigh number should be the same as the force fields of the different configurations are not dynamically similar. The main conclusion to be drawn from this figure should be that all configurations show qualitatively similar behaviour.

An attempt at a quantitative comparison between all cases is presented in Fig. 13 which shows the Nusselt number at the end of each integration against the reference Rayleigh number. Since the flow in some cases appears far from equilibrium, and the choice of the Rayleigh number is somewhat arbitrary, the figure has to be taken as an indication rather than proof. The open circles, joined by the dotted line, are the results for the benchmark configuration A, where the low Rayleigh numbers correspond to the radially increasing fields. The triangle is the case of natural convection under terrestrial gravity only.

The blue stars in Fig. 13 are for the configuration B, and the square and diamond for configuration C. All cases including thermomagnetic convection exceed the benchmark significantly. Any variation of the field in latitude is hidden but is likely to lead to some spots of higher local Rayleigh number which may lead to preferential formation of plumes and increase the effective heat transfer. Another phenomenon, also pointed out by Früh (2005) is the enhancement of convection due to the fact that the Kelvin force tends to have a component perpendicular to the imposed temperature gradient. The perpendicular component will result in convection analogous to that of a cavity heated from the side. Unlike Rayleigh-Bénard convection, which only sets in above a critical Rayleigh number, a large-scale circulation occurs up for any non-zero value of the Rayleigh number and tends to result in a higher Nusselt number than Rayleigh-Bénard convection.

## 5 Discussion of approach

The results have demonstrated that thermomagnetic convection can be used to simulate a largely radially aligned force field. Due to the spatial structure of the magnetic field, this force field shows some deviation from rotational symmetry where the magnitude of the deviation depends on the arrangement of the magnets. The similar system of convection in a spherical capacitor does not show this imperfection but it is limited both, to a single type of radial variation of the force field, and in magnitude as it is difficult overcome terrestrial gravity over a sufficient part of the fluid domain. This restricts such experiments for the investigation of central force fields to microgravity environments, as was used by Hart et al. (1986) and is being taken further by Beltrame et al. (2005)[1]. The approach of using magnets and a magnetic liquid offers more flexibility in the shape of the force field, and it is much easier to generate sufficiently strong magnetic forces. Configuration B was a marginal case, where a clear competition between gravity and magnetic forces resulted in a more complex pattern than was observed for the forces separately. In configuration C, however, the magnetic forces dominated over most (not all!) of the domain, and this configuration did not seem to be susceptible to the presence or absence of terrestrial gravity. The thermomagnetic convection showed somewhat enhanced convection compared to pure central force fields, which was attributed to the deviation from rotational symmetry of the magnetic force field, but the qualitative behaviour was the same as for truly symmetric force fields.

While our system is that of a non-rotating shell, and thus limited in its direct relevance to large-scale geophysical interpretation, it is a first justification for developing this approach further. To substantiate this claim, it is worth comparing the results with other studies of non-rotating convection cells which also point to their geophysical and astrophysical relevance. Li et al. (2005) mention that nonlinear thermal convection in a spherical shell does organise itself into convection rolls which may or may not have a longitudinal modal structure. Since they aimed to uncover systematically the effect of co-existence of multiple solutions, they concentrated on thin shells but mention that such multiplicity reduces as the shell becomes thicker. With a radius ratio of $R_i/R_o$=0.35, the system investigated here is a thick shell, and the solutions found are consistent with hemispherical convection rolls. The experiment by Rosensweig et al. (1999) is almost a direct experimental version of configuration B, though in a much thinner shell with $R_i/R_o$=25 mm/17.5 mm=0.7, between the two cases studied by Li et al. (2005). The experimental results presented a side view of natural convection in water and compared it

**Table 3.** Physical and nondimensional parameters of experimental sequence used for analysis.

| Nondimensional number | | Experiment | Earth's mantle | Earths' core |
|---|---|---|---|---|
| Rayleigh number | $Ra$, Eq. (1), or $Ra_M$, Eq. (3) | $10^7 - 10^9$ | $O(10^8)$ | $> 10^{12}$ |
| Ekman number | $E = \nu/(\Omega D^2)$ | $O(10^{-4})$ | $O(10^{11})$ | $< 10^{-12}$ |
| Prandtl No. | $Pr = \nu/\kappa$ | 14.2 | $O(10^{23})$ | $O(10^{-2})$ |
| Rossby number | $Ro = U/(2\Omega D)$ | $O(10^{-1})$ | $< 10^{-4}$ | $O(10^{-1})$ |
| Reynolds number | $Re = UD/\nu$ | $O(10^3)$ | $< 10^{-15}$ | $O(10^7)$ |

to the top view of thermomagnetic convection for three temperature gradients. As a result, no information on the vertical structure of the thermomagnetic convection could be extracted.

A direct comparison with this experiment and the spherical capacitor can be found in Beltrame et al. (2005)[1] who studied an experiment, to be flown on the International Space Station, in a terrestrial laboratory without background rotation. Since their dielectric Rayleigh number is rather moderate, their calculations result in a single hot plume rising from the top of the core. As the dielectric Rayleigh number is increased, the structure remains largely unaffected but an oscillation was observed. Their oscillation is consistent with the fluctuations found in configuration B with gravity, although the magnetic Rayleigh number in our case was strong enough to dominate the overall flow structure. They argue that the onset of the oscillation is a result of symmetry breaking caused by the superposition of the vertical gravity and the central electric force. This argument would also apply to our case.

## 6 Conclusions

This paper has presented a Finite-Element analysis of a section through a spherical shell, where convection is driven either by a specified central "gravity" or by thermomagnetic convection. The results showed that thermomagnetic convection alone was capable of simulating a central force field, which could either follow a radial decay or a radial increase. We also presented evidence that such thermomagnetic convection could dominate the result if the system were placed into the gravity field of a terrestrial laboratory if sufficiently strong magnets were chosen. If the magnetic forces exceeded gravity over most of the fluid domain, the effect of gravity would be a minor modification but if the force balance was not so clear, the result would be much more complicated.

If this experiment were placed on a rotating platform, operating at a moderate rotation rate of $\Omega \sim 1$ rad/s, then the parameters listed in Table 3 would be achieved. These are clearly no direct match to either the Earth's mantle or core but the ranges of Rayleigh numbers would certainly allow a useful investigation. Designing a somewhat larger and faster system, it could be possible to reduce the available Ekman number by two orders of magnitude, providing a system which could provide useful insight.

Edited by: J.-B. Flor
Reviewed by: three referees

## References

Amara, K. and Hegseth, J.: Convection in a spherical capacitor, J. Fluid Mech., 450, 297–316, 2002.

Aurnou, J., Andreadis, S., Zhu, L., and Olson, P.: Experiments on convection in Earth's core tangent cylinder, Earth Planet. Sci. Lett., 212, 119–134, 2003.

Beltrame, P., Egbers, C., and Hollerbach, R.: The GEOFLOW-experiment on ISS (Part III): Bifurcation analysis, Adv. Space Res., 32, 191–197, 2003.

Egbers, C., Beyer, W., Bonhage, A., Hollerbach, R., and Beltrame, P.: The GEOFLOW-experiment on ISS. I: Experimental preparation and design of laboratory testing hardware, Adv. Space Res., 32, 171–180, 2003.

Früh, W.-G.: Heat transfer enhancement by thermomagnetic convection, in: Sustainable (Bio)Chemical Process Technology, edited by: Jansens, P., Stankiewicz, A., and Green, A., 47–56, BHR Group Ltd., 2005.

Gubbins, D.: The Rayleigh number for convection in the earth's core, Phys. Earth Planet. Interiors, 128, 3–12, 2001.

Hart, J. E., Glatzmaier, G. A., and Toomre, J.: Space-laboratory and numerical simulations of thermal convection in a rotating hemispherical shell with radial gravity, J. Fluid Mech., 173, 519–544, 1986.

Huppert, H. E.: Geological fluid mechanics, in: Perspectives in Fluid Dynamics, edited by: Batchelor, G. K., Moffat, H. K., and Worster, M. G., chapt. 9, 447–506, Cambridge University Press, 2000.

Li, L., Zhang, P., Liao, X., and Zhang, K.: Multiplicity of nonlinear thermal convection in a spherical shell, Phys. Rev. E, 71, 016 301–1–9, 2005.

Moffatt, H. K.: Reflections on magnetohydrodynamics, in: Perspectives in Fluid Dynamics, edited by Batchelor, G. K., Moffatt, H. K., and Worster, M. G., chapt. 7, 347–391, Cambridge University Press, 2000.

Ohlsen, D. R. and Rhines, P. B.: Laboratory studies of equatorially trapped waves using ferrofluid, J. Fluid Mech., 338, 35–58, 1997.

Rosensweig, R. E.: Ferrohydrodynamics, Cambridge University Press, 1985.

Rosensweig, R. E., Borwaeys, J., Bacri, J.-C., Zebib, Z., and Perzynski, R.: Laboratory study of spherical convection in simulated central gravity, Phys. Rev. Lett., 83, 4904–4907, 1999.

Travnikov, V., Egbers, C., and Hollerbach, R.: The GEOFLOW-experiment in ISS. II: Numerical simulation, Adv. Space Res., 32, 181–189, 2003.